RSC Advances




ROYAL SOCIETY OF CHEMISTRY

www.rsc.org/advances

Cite this: DOI: 10.1039/c0xx00000x

www.rsc.org/xxxxxx

ARTICLE TYPE

# Controlled synthesis of porous $Co_3O_4$-C hybrid nanosheet arrays and their application in lithium ion batteries

**Jun Wang,[a,b] Bing Gao[a], Long Zhang[b], Rui Li[b], Jinpeng Shen[b], Zhiqiao Qiao[a], Guangcheng Yang*[a, b] and Fude Nie[a]**

***Received (in XXX, XXX) Xth XXXXXXXXX 20XX, Accepted Xth XXXXXXXXX 20XX***
**DOI: 10.1039/b000000x**

Two-dimensional $Co_3O_4$ nanostructures with porous inside architecture are experiencing rapid development in the functional material fields for their unique structures and properties. Porous $Co_3O_4$-C hybrid nanosheet (NS) arrays grown directly on various conducting substrates are controlled synthesized for the first time via a facile hydrothermal synthesis approach in combination with the heat treatment. These NS arrays reveal uniform hexagon morphology and have combined properties of quasi-single-crystallinity and pore-network inside the architecture. A four-step formation mechanism is proposed to understand the growth process of the nanosheet arrays grown on the substrate based on the change of morphology. Both the concentration of $Co^{2+}$ and poly(vinylpyrrolidone) (PVP) play key roles in the formation of NS arrays. When tested as the anode material in lithium-ion batteries, the porous $Co_3O_4$-C hybrid NS arrays exhibit improved electrochemical properties of cyclic performance and high coulombic efficiency compared with the commercial $Co_3O_4$ and $Co_3O_4$/carbon nanocomposites. This approach, porous $Co_3O_4$-C NS arrays grown directly on different substrates (wafer, foam, alloy net, foil, especially flexible carbon cloth), provides an efficient way to produce NS arrays to meet the demand for diversity and may be extended to synthesize other transition metal oxide materials for other applications.

## 1 Introduction

Because of the unique structures and properties, two-dimensional (2D) metal oxide nanostructures have aroused growing interest in functional materials[1-3] and application in energy storage devices such as the electrode materials for supercapacitor and lithium-ion batteries (LIBs).[4,5] However, low conductivity and surface area of these 2D metal oxide nanosheets have dramatically reduced their actual capacitance performance such as cycle stability and rate performance in LIBs.

Viewing these disadvantages, lots of efforts have been devoted to increase the conductivity and surface area of the nanosheets. One effective way is to grow directly those self-supported nanosheets (such as $Fe_2O_3$,[6,7] $MnO_2$,[8,9] NiO[11,12] and CuO[13,14] arrays) arrays on the substrate. It could increase the electrical contact between electrode materials and collector (the subtracts) to provide much better whole conductivity. Furthermore, for the high surface area, porous structure is introduced inside the nanostructure arrays to achieve enhanced reactivity because of the high porosity could facilitate the access of guest molecule/ion into the active particles.[15-17] Moreover, Synthesis $Co_3O_4$-C composite is a good way to improve the electrochemical property of pure $Co_3O_4$. The doped carbon can not only provide a flexible buffer to accommodate the volume change during lithium insertion/extraction, but also can increase the conductivity of the electrode.[18-24] Therefore, porous NS arrays doped carbon on the substrate have exhibited great promising application on lithium-ion. And for wider application and the demand for diversity, a universal strategy should be developed to synthesis porous NS arrays doped carbon for more common conducting substrates.

Considering all these above, we studied the direct synthesis of porous $Co_3O_4$-C hybrid NS arrays on various conducting substrates, using a simple hydrothermal approach in combination with heat treatment. $Co_3O_4$ nanosheets is used due to the relatively low environmental footprint, low-cost, and the high theoretical capacity for LIBs (890 mA h $g^{-1}$).[25-29] And carbon is doped to $Co_3O_4$ by adding poly(vinylpyrrolidone) (PVP) in the precursors. Carbon not only introduces porous structure to achieve higher surface area, but also further increases the conductivity of the electrode. The $Co_3O_4$-C hybrid NS arrays show hexagons in morphology with most of the sheets lying aslant or perpendicular to the substrate. Furthermore, based on time-dependent experiment results, a possible formation mechanism for this nanosheet arrays is proposed. Compared with commercial $Co_3O_4$ and $Co_3O_4$/carbon nanocomposites, much better electrochemical properties of rate performance and high coulombic efficiency are observed when using the porous $Co_3O_4$-C hybrid NS arrays on Ni substrates as electrode materials. The facile method, along with the wide applicability to many conducting subtracts and good electrochemical properties indicate

that our method is highly promising for the synthesis of porous metal oxide nanosheets for many applications.

## 2 Experimental

### 2.1 Synthesis of $Co_3O_4$-C nanosheet arrays on substrates

All of the reagents were analytically pure, and were purchased from the Aladdin reagent (Shanghai, China) Co, LTD.; they were used without further purification.

In a typical procedure, 0.50-2.00 g of $Co(CH_3COO)_2{\cdot}4H_2O$ and 0.50-0.80 g poly(vinylpyrrolidone) (PVP Mw=30000) were added into 40-60 ml ethylene glycol within 30 min with magnetic stirring. The whole mixture was then transferred into a Teflon-lined autoclave and maintained at 160 °C for 18 h, then cooled down to room temperature naturally. Before being transferred into the Teflon-lined autoclave, the substrates (Silicon wafer; Ni foam; copper foils; carbon cloth) were put into the autoclave. The substrates were cleaned using different method. After reaction, the substrates were thoroughly washed with deionized water and ethanol 4-6 times each, and dried in an oven at 60 °C for 2 h. Finally, the samples were annealed at 450 °C for 2-4 h a $N_2$ flow, and then cooled down to room temperature naturally.

### 2.2 Characterizations

The as-prepared precursors and products were characterized by powder XRD using X'Pert PRO X-ray diffractometer with monochromatized Cu Kα (λ=1.54059Å) incident radiation and Fourier transform IR (FTIR) spectroscopy (Nicolet-5700, Nicolet Co., USA). The morphologies and structures of all the products were analyzed by FE-SEM (Ultra 55), TEM and SAED (Libra 200FE operated at 200 kV). The Raman spectrum was taken using a micro-Raman/Photo-luminescence system (In Via). X-ray photoelectron spectra (XPS) data was recorded by a Multilab-2000 electron spectrometer using acrochro-matic Al Kα radiation (1486.6 eV). The specific surface area was calculated by multipoint Braunauer-Emmett-Teller (BET) analysis of the nitrogen desorption isotherm.

### 2.3 Electrochemical Test

Half cells were assembled for measuring the electrochemical performance of $Co_3O_4$-C NS arrays, in which the as prepared $Co_3O_4$-C NS arrays were used as working electrode and a lithium plate as counter electrode. As a typical example, the different as-prepared $Co_3O_4$-C NS arrays were heated at 150 °C for 1 h before the sheet was pressed and punched into 1 cm diameter electrodes. The coin-type cells were assembled in a glove-box filled with pure argon (99.999%), and 1 M $LiPF_6$ dissolved in 1:1:1 (v/v/v) mixture of ethylene carbonate/diethyl carbonate/dimethyl carbonate (EC/DEC/DMC) were employed as the electrolyte. The cells were tested on an Arbin® BT2000 battery testing system between 3.0 V and 0.01 V (vs. Li) at ambient temperature (25 °C).

## 3 Results and discussion

Ni foam is chosen as the substrate due to its high electrical conductivity and a desirable 3D porous structure. In this work, self-supported porous $Co_3O_4$-C hybrid nanosheet (NS) arrays in the large area directly grown on Ni foam and silicon substrate are synthesized successfully by a facile hydrothermal method in combination with heat treatment. The contents of $Co(CH_3COO)_2{\cdot}4H_2O$ and PVP are 2.0 g and 0.8 g, respectively. Fig. 1(a) shows field-emission scanning electron microscope (FE-SEM) images of the hexagon shaped precursor of NS arrays on the substrate. It can be clearly observed that large-scale $Co_3O_4$ arrays uniformly grow on the substrate with a relatively high density. Besides, most of the sheets lie aslant or perpendicular on the substrate with one edge anchored. As shown in Fig. 1(b), the morphology of the sample before and after annealing at 450 °C for 2 h in $N_2$ flow still maintains array structures. The FE-SEM images reveal that NS are hexagons with regular edges, and hexagons with average edge length of 1-1.5 μm and a thickness about 100 nm. More interestingly, the surface of the precursor is smooth and compact (Fig. 1(a)), however, the surface of the sheets after annealing is full of dark points (the inset of (b)). This results reveal that these NS have obvious porous-like inside architecture. The pores inside structures are formed due to the decomposition of the PVP and dehydration during thermal treatment. The cross-sectional SEM image shown in Fig. 2(c) reveals that the $Co_3O_4$ NS arrays with a height of about 3 μm are homogeneously aligned on the substrate. The height of the nanosheet can be controlled by the hydrothermal time in our experiment. Fig. 1(d)-(e) show FE-SEM images of $Co_3O_4$-C NS arrays on Ni foam. The FE-SEM images reveal that porous $Co_3O_4$ NS arrays grown directly on the Ni foam have been synthesized successfully.

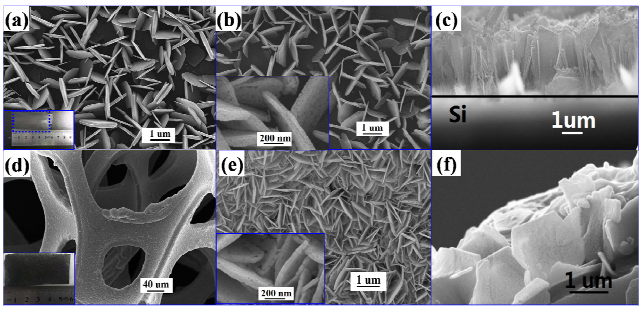


Fig.1 FE-SEM images of NS arrays on silicon substrate. (a) before and (b) after annealing at 450 °C for 2 h in $N_2$ flow, which show high porous structure after annealing. The inset of (a) shows optical image of precursor NS arrays on silicon. (c) FE-SEM image of a cross section region in (b). Low (d) and high (e) FE-SEM images of NS arrays on Ni foam after annealing at 450 °C for 2 h in $N_2$ flow. The inset of (d) shows optical image of Ni foam after annealing. (f) FE-SEM image of a cross section region in (d). Both Fig.1(c) and Fig.1(f) indicate that the $Co_3O_4$-C hybrid NS arrays show hexagons in morphology with most of the nanosheets lying aslant or perpendicular to the substrate.

Fig. 2(a) shows the XRD patterns of the precursor and the final products scraped off from the substrate, and the products were prepared by annealing at 450 °C for 2 h in $N_2$ flow. Compared to the precursor, the XRD pattern of obtained products consists of nine diffraction peaks attributed to the (111), (220), (311), (222), (400), (422), (511), (440) and (533) planes of the $Co_3O_4$ phase (JCPDS card No. 42-1467), respectively. There are no diffraction peaks from any other impurities, which indicate that the high purity of $Co_3O_4$ has been formed by annealing the precursor. The FTIR and the Raman spectrum of the products also supported. In FTIR spectra of obtained products (Figure. S1), two very strong peaks centred at 576 and 672 $cm^{-1}$ are noticed. The Raman

spectrum (Figure. S2) displays four Raman peaks located at

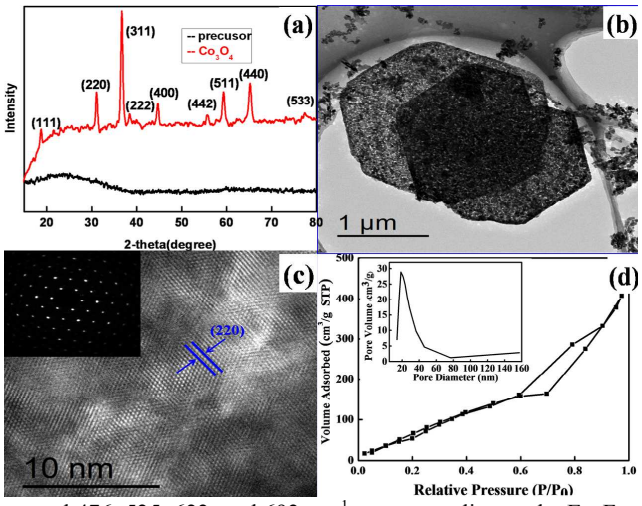


around 476, 525, 622, and 692 $cm^{-1}$, corresponding to the $E_g$, $F_{2g}$, $F_{2g}$, and $A_{1g}$ modes of the $Co_3O_4$ phase, respectively. [30]

Fig.2 (a) XRD patterns of precursor and porous $Co_3O_4$-C NS scraped off from the substrate. (b) TEM image of the porous $Co_3O_4$-C NS. (c) HRETM image of the porous $Co_3O_4$-C NS. The inset of (c) shows SAED pattern of the porous $Co_3O_4$-C NS is quasi-single-crystalline in nature. (d) Typical nitrogen-adsorption-desorption isotherm, BET surface area and pore-size distribution (inset) of the $Co_3O_4$-C hybrid NS, which indicat the existence of abundant pores 13 to 20 nm in diameter.

A typical TEM image (Fig. 2(b)) indicates that a single sheet has an edge length of 1.5 μm and porous structure, which agrees with FE-SEM observations. The magnified HRTEM image (Fig. 2(c)) analysis reveals that nanosheet demonstrate highly oriented growth. The SAED analysis further indicates that the $Co_3O_4$ is quasi-single-crystalline in nature (The inset of (c)). No SAED patterns of carbon are observed implying its amorphous nature, which is in agreement with the XRD pattern. Besides, the nanosheets have a highly porous texture, which may be formed due to the decomposition of PVP and dehydration occurring during the thermal treatment. These results reveal that porous $Co_3O_4$-C NS arrays on the substrate with quasi-single-crystalline have been achieved. The porous structure of the $Co_3O_4$-C hybrid NS arrays was further evaluated by Brunauer-Emmett-Teller (BET) $N_2$-adsorption-desorption analysis. Fig. 2(d) shows the adsorption-desorption isotherm and pore-size-distribution plot of the $Co_3O_4$-C hybrid NS. The loop observed was ascribed as a type-H3 loop, indicating the existence of abundant pores 13 to 20 nm in diameter. While the size and shape of the pores are not uniformed, most of them are around 21.3 nm in diameter (pore volume: 17.37 $cm^3g^{-1}$). The BET surface area of the material is 28.93 $m^2g^{-1}$.

More detailed compositions of the porous $Co_3O_4$-C NS are further characterized by X-ray photoelectron spectroscopy (XPS) and energy dispersive X-ray (EDS) spectrum. The contents of $Co(CH_3COO)_2{\cdot}4H_2O$ and PVP are 2.0 g and 0.8 g, respectively. The corresponding results are presented in Fig. 3. XPS spectrum consists of O, Co, and C. The Co 2p XPS spectrum (Fig. 3(b)) shows two major peaks with binding energies at 779.6 and 794.7 eV, corresponding to Co $2p_{3/2}$ and Co $2p_{1/2}$, respectively, with a spin-energy separation of 14.9 eV, which is characteristic of a $Co_3O_4$ phase.[26,27] The result is well consistent with the XRD data.

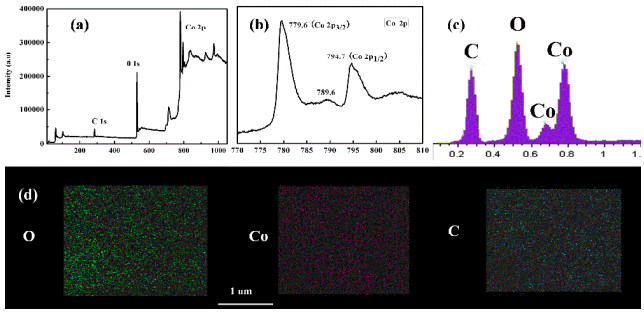


Fig. 3(a) XPS spectrum of the porous $Co_3O_4$-C NS. (b) Co 2p Xp spectrum obtained on the porous $Co_3O_4$-C NS. (c) EDS elemental intensity of $Co_3O_4$-C NS. (d) The mapping of each element corresponding to O, Co, C, respectively. The content of carbon in $Co_3O_4$ NS arrays is 15.2%.

Energy dispersive X-ray (EDS) spectra (Fig. 3(c)) analysis clearly show the existence of elemental Co, O and C with an atomic ratio of Co to O in excess of 3:4. As supplement information for the chemical analysis of the composites, EDX element maps are collected by scanning the one side area of $Co_3O_4$-C NS. Fig. 3(d) shows the images of each element corresponding to O, Co, and C, respectively. The elemental maps confirm that each element (O, Co, C) is homogeneously distributed in $Co_3O_4$-C hybrid NS. The content of carbon is further characterized by thermogravimetric analysis (TG-DSC, Fig.4) of precursor and final products. A total weight loss of 29.7% ranging from 240-260 °C in air is attributed to the decomposition of the PVP and glycolate group (Fig.4(a)). Compared to the precursor, a weight loss of 14.5% of the final product (Fig.4(b)) is obtained by the loss of carbon. More importantly, the carbon content of $Co_3O_4$-C NS can be controllable synthesized through controlling concentration of PVP in the precursor and treatment conditions. The carbon content rings from 21.30 % to 5.30 % in $Co_3O_4$-C hybrid structure (Figure. S3). The carbon would provide a flexible buffer to accommodate the volume change during lithium insertion/extraction and increase the conductivity of the electrode. Therefore, it is highly significant to control the carbon content in electrode materials for the improving electrochemical properties of lithium-ion batteries.

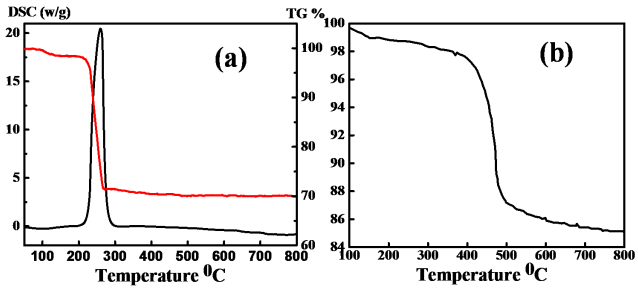


Fig.4 TG-DSC curves of samples scraped off from the substrate. (a):precursor, (b): $Co_3O_4$-C NS after annealing at 450 °C for 2 h in $N_2$ flow, which show the content of carbon in in $Co_3O_4$ NS arrays is 14.5%.

A four-step growth mechanism concerning the growth of $Co_3O_4$-C NS arrays on the substrate is proposed based morphology and literatures[30-34] (Fig.5). First: bivalent $Co^{2+}$ ions are fully coordinated with EG to form cobalt glycolate in the as-prepared homogeneous solution during magnetic stirring. Cobalt

glycolate unit comprises one cobalt atom and one coordinated ethylene glycol. The transformation of cobalt acetate to cobalt glycolate is also supported by FTIR analysis (Figure. S1). Second: with the temperature of the reactant solution ramped in the oven, the reaction between PVP and cobalt glycolate leads to the formation of a nucleus on the substrate (fig. 5(a)). Third: Due to the continuously proceeding reaction, the growing nuclei are beginning to assemble along the specific orientation preferentially to form nanosheets (fig. 5(b)) and further grow perfect hexagon morphology (fig. 5(c)). Finally, after annealing at 450 °C for 2 h in $N_2$ flow, the precursor decomposed gradually and black $Co_3O_4$-C NS arrays with pores are obtained (fig. 5(d)).

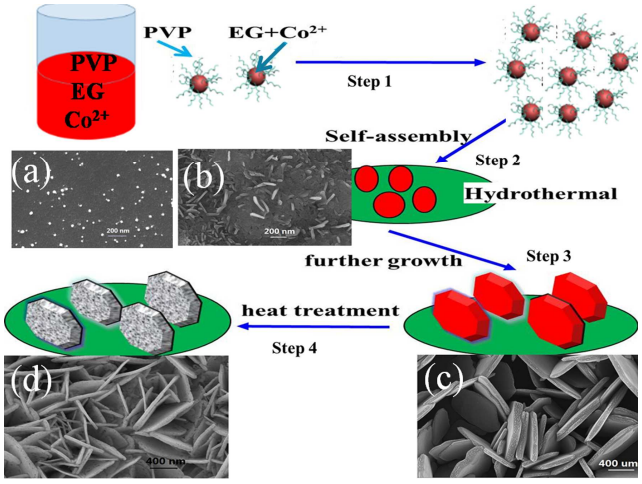


Fig. 5 Schematic diagrams of the formation process of $Co_3O_4$-C NS arrays by a hydrothermal synthesis approach and heat treatment. (a) FE-SEM image of precursor on substrate at the initial stage. (b) FE-SEM image of precursor on substrate at the intermediate stage. (c) FE-SEM image of precursor on substrate at the final stage. (d) FE-SEM images of porous $Co_3O_4$-C hybrid NS arrays on silicon substrate after annealing at 450°C for 2 h in $N_2$ flow.

To achieve well-defined structure of the synthesized $Co_3O_4$-C NS arrays, the effect of experimental parameters (cobalt ion and PVP) on the nanosheet arrays are investigated. The concentration of the cobalt ion solution is varied from 5 to 80 mM when other conditions are kept constant. Fig.6 present field-emission scanning electron microscopy (FE-SEM) images of NS. From these images, one can see the features: 1) the porous $Co_3O_4$-C NS with irregular hexagon mostly lie low on the substrate, only few sheets are perpendicular to the substrate with low concentration of cobalt ion. 2) The freestanding porous $Co_3O_4$-C NS arrays formed with concentration increased, the sheets have regular hexagon in morphology. 3) With continuously increasing concentration, the substrate is completely covered by porous $Co_3O_4$-C NS arrays, which grow densely and almost vertically from the substrate. Fig. 6(d) shows the unordered morphology of products grown on the substrate without PVP. The results suggest that the concentration ($Co^{2+}$) and PVP are important key parameters affecting the formation of NS arrays. Therefore, ordered and aligned porous $Co_3O_4$-C NS arrays are fabricated through controlled the conditions of the reaction.

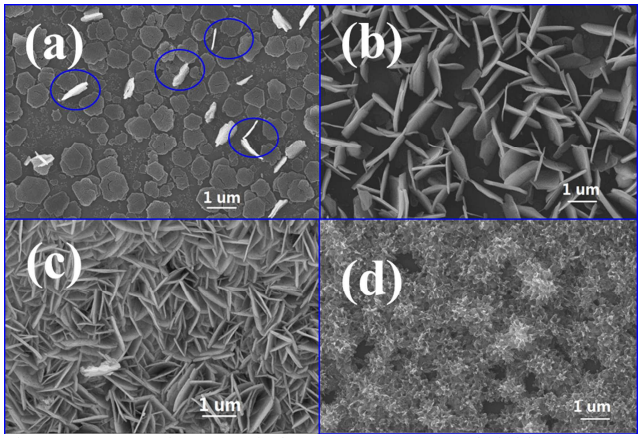


Fig. 6 FE-SEM images of the porous $Co_3O_4$-C hybrid NS arrays synthesized at different conditions: (a) 5 mM cobalt ion, (b) 30 mM cobalt ion, (c) 80 mM cobalt ion, (d) 30 mM cobalt ion without PVP.

In order to promote this technology and extended to more common substrates to meet the demand for diversity. The bendable ability of metallic foils without degradation of the active materials grown on them enables the as-made energy storage device to be potentially applied in the field of flexible electronics. Fe-Cr alloy net and copper foils with low cost are the most commonly used as current collecting substrate. As a highly flexible, carbon cloth consisting of carbon fibers orienting in two directions shows some unique properties, such as high strength, high conductivity, and good corrosion resistance. Recently, carbon cloth has been a promising conducting substrate without using any insulating binders. However, to the best of our knowledge, there not many reports on the fabrication of porous $Co_3O_4$-C hybrid NS arrays on carbon cloth via a hydrothermal method followed by annealing[35-36]. Therefore, it is worthwhile to synthesis the porous $Co_3O_4$-C NS arrays on those conducting substrate. Fig. 7 show the morphologies on different substrates, and some different exist in morphology of NS. To the best of our abilities, the yield of distinguishing in structures could be attributed to the intrinsic properties and shapes of the substrates. However, the substrates can affect the structures of NS to some extent but not alter the general morphology of NS.

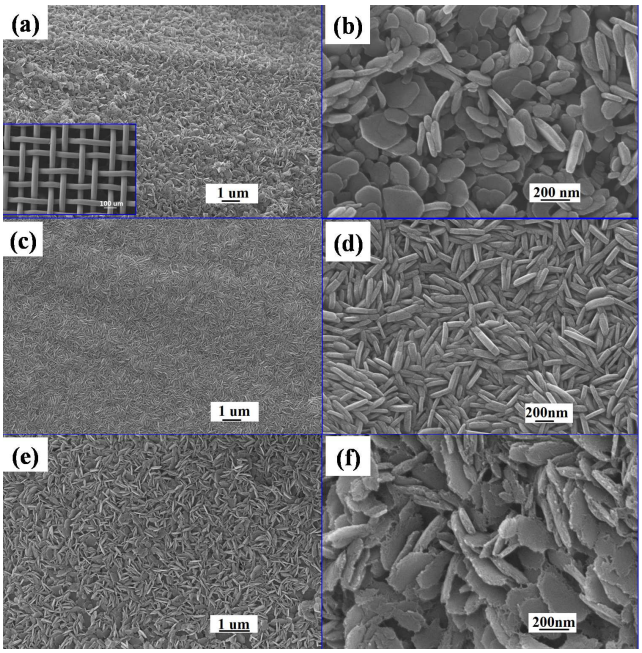


Fig. 7 The precursor NS arrays on different substrate. (a) and (b) on Fe-Cr alloy net, (c) and (d) on copper foils, (e) and (f) on carbon cloth. The morphology display some difference on different substrate, the substrates can affect the structures of NS to some extent but not alter the general morphology of NS.

Based on the combined properties of the porous structure, high theoretical capacity (890 mA h $g^{-1}$) for lithium-ion batteries and intense contact between $Co_3O_4$-C hybrid arrays and the conducting substrate, we use the porous $Co_3O_4$-C hybrid NS arrays on Ni foam as an anode material for lithium-ion batteries. The charge/discharge performance of the 1st, 2nd, 5th and 25th cycles is shown in Figure. 4S. The sample was synthesized using 2.00 g $Co(CH_3COO)_2 \cdot 4H_2O$ and 0.60 g PVP, and annealed at 450 °C for 2-4 h $N_2$ flow. The carbon of the sample is 14.5% tested by TG-DSC. The capacity is based on the mass of $Co_3O_4$-C composite. The first cycle reversible specific capacity of the porous $Co_3O_4$-C hybrid NS arrays is as high as 850 mA h $g^{-1}$, which is close the theoretical capacity of 890 mA h $g^{-1}$. The reversible capacity of the $Co_3O_4$-C hybrid NS arrays at the 25$^{th}$ cycle is 846.4 mA h $g^{-1}$, higher than that of the $Co_3O_4$ NS array in previous reports.[37,38] In comparison, the capacity of the commercial $Co_3O_4$ sample and $Co_3O_4$/C nanocomposites (80-100 nm in size) is severely fade after only 20 cycles (Figure. 5S(a) and (c)), which demonstrates that the porous $Co_3O_4$-C hybrid NS arrays have much better cycle performance. In order to further display the cycling performance of $Co_3O_4$-C nanosheet arrays, the charge capacity and the columbic efficiency with cycling at a current rate of C/2 is tested (Figure. 5S(b)). The capacity of $Co_3O_4$-C nanosheet arrays remain as high as 720 mA h $g^{-1}$, after 50 cycles. The corresponding fading rate is 1.2% per cycle. It is evident that $Co_3O_4$-C nanosheet arrays show much good cycling performance. The results indicate that the unique structures together with doped carbon in $Co_3O_4$ not only can improve the electrochemical performance of $Co_3O_4$, but also can significantly increase the work stability of the electrodes, as well as the rate for ion diffusion and electron transportation in lithium-ion batteries.[21-23]

The rate performance of several $Co_3O_4$-C NS arrays with different carbon content are tested at different current densities as shown in Fig. 8. It can be seen that even at a high current density of 2C, this material can still deliver a capacity of 571 mA h $g^{-1}$ (Fig.8(a)). And when the current density changed back from 2C to 0.2C, the capacity also increased from 571 mA h $g^{-1}$ to 840 mA h $g^{-1}$, which is equal to the capacity at the current density of 0.2C for the first five cycles. Fig. 8 also reveals the capacity of $Co_3O_4$-C NS arrays depended on carbon content. With the carbon content decrease from 16.5 to 5.6%, the capacity of $Co_3O_4$-C NS decreases from 840 to 652 mA h $g^{-1}$ for the same 25$^{th}$ cycle, indicating great influence of carbon content for the electrochemical performance of $Co_3O_4$ NS arrays. The doped carbon could increase the electrode-electrolyte interface stability, the conductivity of the electrode and effectively buffer the volume change of $Co_3O_4$ during lithium ion insertion/extraction, leading to improve electrochemical properties.[39]

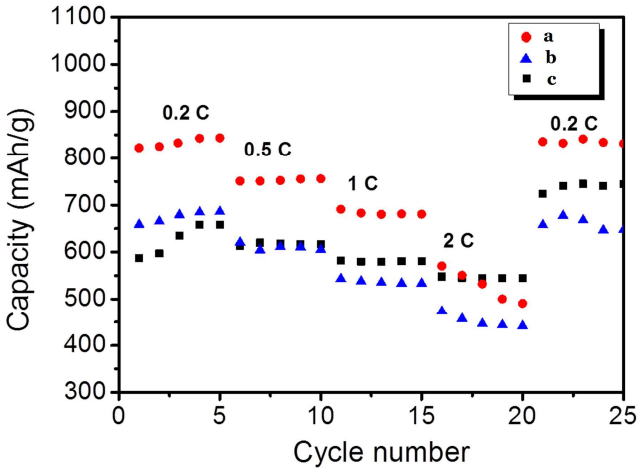


Fig. 8 Rate capability of $Co_3O_4$-C NS arrays electrodes with different carbon content. The carbon content of a, b and c is 16.5%, 9.7% and 5.6%, respectively.

The unique structure of porous $Co_3O_4$-C hybrid NS arrays has the following important merits required for high-performance electrodes. The open space between the NS and pores existing in the architecture can facilitate the fast penetration of the electrode. Moreover, the direct contact of each NS to the underlying conductive substrate avoids the use of a polymer binder and conductive additives, and substantially reduces the "dead volume" in the electrode. Finally, uniformly distributed carbon in $Co_3O_4$ NS not only greatly enhances the surface conductivity and the electrical contact in the electrode, but also effectively buffers the large volume expansion during the ion insertion process.

## 4 Conclusions

In summary, porous $Co_3O_4$-C hybrid nanosheet (NS) arrays grown directly on various conducting substrates have been synthesized successfully using a simple method. The $Co_3O_4$-C NS have combined properties of quasi-single-crystallinity and pore-network with inside the architecture, which help to achieve improved performance in lithium-ion batteries. The experimental results reveal that both the concentration of PVP and $Co^{2+}$ play dramatically roles in generating NS arrays. A four-step growth mechanism is proposed to explain the formation of the NS arrays

on the substrate. Based on the four-step growth proposed, other transition metal oxide ordered nanosheet arrays on various substrates to meet the demand for diversity.

## Acknowledgements

The present research was supported by the National Natural Science Foundation of China (No. 11172292, 11172276, 11172275, 11372288). Science Foundation for Young Scientist of Sichuan Province (2012JQ0038). Institute of Chemical Material Fund (QNRC-201201).

## Notes and references

[a] *Institute of Chemical Materials, China Academy of Engineering Physics,No. 64, Mianshan Road, Mianyang City, China. Fax: (86) 8162544426; Tel: (86) 8162482005; E-mail: ygcheng@hotmail.com*

[b] *Sichuan New Material Research Center, No.20, yuan yi street, Mianyang, China. Tel: (86) 8162544436; E-mail: wjnjun@163.com*

† Electronic Supplementary Information (ESI) available: [FTIR curves of the precursors and products, Raman spectrum of products, EDX spectrum of products with different carbon, FE-SEM images of the porous $Co_3O_4$-C hybrid NS arrays synthesized at different conditions, FE-SEM images of NS arrays on different substrate]. See DOI: 10.1039/b000000x/

1 X. Huang, S. Tang , X. Mu, Y. Dai, G. Chen, Z. Zhou, F. Ruan, Z. Yang and N. Zheng, Nat. Nanotechnol.,2011,6,28-31.
2 M. R. Waller, T. K. Townsend, J. Zhao, E. M. Sabio, R. L. Chamousis, N. D. Browning and F. E. Osterloh, Chem. Mater., 2012, 24, 698-704.
3 M. Chhowalla, H. S. Shin, G. Eda, L. J. Li, K. P. Loh and H. Zhang, Nat. Chem., 2013,5,263-275.
4 R. Wang, C. Xu, J. Sun, Y. Liu, L. Gao and C. Lin, Nanoscale, 2013, 5, 6960-6967.
5 S. Q. Chen and Y. Wang, J. Mater. Chem., 2010, 20, 9735-9739.
6 H. Wu, M. Xu, Y. Wang and G. Zheng, Nano. Res.,2013, 6,167-173.
7 D. Lei, M. Zhang, B. Qu, L. Chen, Y. Wang, E. Zhang, Z. Xu, Q. Li and T. Wang, Nanoscale, 2012, 4, 3422-3426.
8 A. M. Reddy, M. M. Shaijumon, S. R. Gowda and P. M. Ajayan, Nano. Lett., 2009, 9,1002-1006.
9 D. Liu, B. B. Garcia, Q. Zhang, Q. Guo, Y. Zhang, S. Sepehri, G. Cao, Adv. Funct. Mater., 2009, 19,1015-1023.
10 J. Jiang, J. Liu, R. Ding, X. Ji, Y. Hu, X. Li, A. Hu, F. Wu, Z. Zhu and X. Huang, J. Phys. Chem. C, 2010, 114,929-932.
11 X. Wang, Z. Yang, X. Sun, X. Li, D. Wang, P. Wang and D. He, J. Mater. Chem., 2011,21, 9988-9990.
12 M. C. Qiu, L. W. Yang, X. Qi, J. Li and J. X. Zhong, ACS Appl. Mater. Interfaces, 2010, 2,3614-3618.
13 X. Chen, N. Zhang and K. Sun, J. Mater. Chem., 2012,22, 13637-13642.
14 X. Huang, S. Tang , X. Mu, Y. Dai, G. Chen, Z. Zhou, F. Ruan, Z. Yang and N. Zheng, Nat. Nanotechnol.,2011,6,28-31.
15 C. Liu, F. Li, L. P. Ma and H. M. Cheng, Adv. Mater., 2010, 22, E28.
16 X. Xia, J. P. Tu, X. L. Wang, C. D. Gu and X. B. Zhao, Chem. Commun., 2011,47, 5786-5788.
17 D.W. Wang, Q. H. Wang, T. M. Wang, Inorg. Chem., 2011, 50, 6482-6492.
18 Z. S. Wu, W. C. Ren, L. Wen, L. B. Gao, J. P. Zhao, Z. P. Chen, G. M. Zhou, F. Li and H. M. Cheng, ACS Nano, 2010, 4, 3187-3181.
19 S. Xiong, J. S. Chen, X. W. Lou and H. C. Zeng, Adv. Funct. Mater. 2012,22, 861-871.
20 J. Sun, H.i Liu, X. Chen, D. G. Evans and W. Yang, Nanoscale, 2013,5, 7564-7571.
21 P. Zhang, Z. P. Guo, Y. D. Huang, D. Z. Jia and H. K. Liu, J. Power Sources, 2011, 196, 6987-6982.
22 J. Chen, X. Xia, J. Tu, Q. Xiong, Y. X. Yu, X. Wang and C. Gu, J. Mater. Chem., 2012, 22, 15056-15061.
23 J. Liu, Y. Wan, C. Liu, W. Liu, S. Ji, Y. Zhou and J. Wang, Eur. J. Inorg. Chem., 2012, 3825-3829.
24 Y. T. Zhong, X. Wang, K. Jiang, J. Y. Zheng, Y. Guo, Y. Ma and J. Yao, J. Mater. Chem., 2011,21, 17998-18002.
25 Y. Li, B. Tan and Y. Wu, Nano. Lett., 2008, 8, 265-270.
26 K. T. Nam, D.W. Kim, P. J. Yoo, C. Chiang, N. Meethong, P. T. Hammond, Y. Chiang and A. M. Belcher , Science, 2006, 312, 885-888.
27 W. Mei, J. Huang, L. Zhu, Z. Ye, Y. Mai and J. Tu, J. Mater. Chem., 2012, 22, 9315-9321.
28 X.Y. Xue, S. Yuan, L. L. Xing, Z. H. Chen, B. He and Y. J. Chen, Chem. Commun., 2011, 47, 4718-4720.
29 Y. Q. Fan, H. Shao, J. Wang, L. Liu, J. Zhang and C. Cao, Chem. Commun., 2011, 47,3469-3471.
30 Q. Yan, X. Li, Q. Zhao, G. Chen, J. Hazard. Mater., 2012,209-210,385-391.
31 A. M. Cao, J. S. Hu, H. P. Liang, W. Song, L. Wan, X. He, X. Gao and S. H. Xia. J. Phys. Chem. B, 2006,110,15858-15863.
32 X. Wang, X. L. Wu, Y. G. Guo, Y. Zhong, X. Cao, Y. Ma and J. Yao, Adv. Funct. Mater., 2010, 20, 1680-1686.
33 X. Wang, H. Guan, S. M. Chen, H. Q. Li, T. Y. Zhai, D. M Tang, Y. Bando, D. Golberg. Chem. Commun., 2011, 47, 12280-12282.J. Xu,
34 J. Jiang, J. P. Liu, X. T. Huang, Y. Y. Li, R. M. Ding, X. X. Ji, Y. Y. Hu, Q. B. Chi, Z. H. Zhu. Cryst. Growth Des., 2009: 10, 70-75.C.
35 Q. F. Wang, X. W. Wang, Q. Y. Xiang, B. Liang, D. Chen, G. Z. Shen. ACS Nano, 2013, 7, 5453-5462.
36 Cheng, G. Zhou, J. Du, H. M. Zhang, D. Guo, Q. H. Li, W. F. Wei, L. B. Chen. New Jour. Chem., 2014, 38, 2250-2253.
37 Z. S. Wu, W. C. Ren, L. Wen, L. B. Gao, J. P. Zhao, Z. P. Chen, G. M. Zhou, F. Li and H. M. Cheng, ACS Nano, 2010, 4, 3187-3190.
38 Z. S. Wu, W. C. Ren, L. Wen, L. B. Gao, J. P. Zhao, Z. P. Chen, G. M. Zhou, F. Li and H. M. Cheng, ACS Nano, 2010, 4, 3187-3181.
39 C. C. Li, Q. H. Li, L. B. Chen and T. H. Wang, J. Mater. Chem., 2011,21, 11867-11872.